



Use of *Thymus vulgaris* Extract as Green Corrosion Inhibitor for Bronze in Acid Rain

J. G. Gonzalez-Rodriguez¹ · D. G. Gutierrez-Granda² · A. K. Larios-Galvez¹ · R. Lopez-Sesenes²

Received: 29 March 2022 / Revised: 6 May 2022 / Accepted: 27 May 2022 / Published online: 15 June 2022
© The Author(s), under exclusive licence to Springer Nature Switzerland AG 2022

Abstract

A study on the use of methanolic extract of *Thymus vulgaris* leaves as green corrosion inhibitor for bronze in simulated acid rain has been carried out using gravimetric and electrochemical tests. Electrochemical tests included potentiodynamic polarization curves and electrochemical impedance spectroscopy. Inhibitor concentrations were in the range 0–1000 ppm, whereas testing temperatures included 25, 40 and 60 °C. The results indicate that *T. vulgaris* is a good, anodic type of inhibitor with an efficiency that increased with the inhibitor concentration, reaching its maximum value, higher than 90%, at a concentration of 800 ppm, but it decreased as the temperature increased from 25 down to 60 °C. The inhibitor is physically adsorbed onto the metal surface according to a Langmuir adsorption isotherm at the different testing temperatures. The extract contains many antioxidants being the most abundant ones phenol, 2-metil-5-(1-metilethyl)- and D, α -tocopherol which give to the extract its inhibitory properties.

Keywords Bronze · Acid rain corrosion · Green corrosion inhibitor

1 Introduction

Bronze is a Cu–Sn alloy widely used for sculptures and architectonic structures exposed to the atmosphere due to excellent properties such as hardness, tenacity, malleability and high corrosion resistance [1]. Its high-corrosion resistance is due to a passivating layer formed on top of its surface known as “patina” which protects the alloy from atmospheric [1–4]. However, due to the increase in the emissions of Greenhouse effect gases and the use of fossil fuels, an increase in the acid rain has been observed in last years. When acid rain gets in contact with brass a rapid metal degradation occurs with a subsequent damage of sculptures and architectonic structures [5–7]. One of the most popular ways to fight corrosion is using corrosion inhibitors since they offer an efficient alternative to control metals degradation.

In the last decade, the use of extracts from plants has been widely used to protect metals from corrosion in acidic environments such as acid rain due to many advantages they offer has been reported [8]. These studies reveal that the inhibition properties of these extracts is due to the presence of heteroatoms such as S, O and N as well as to the aromatic rings and conjugated links in their molecular structure [9–13].

BinYehmed et al. [14] studied the green coffee bean extract as corrosion inhibitor for Al in simulated acid rain using potentiodynamic polarization curves. Results showed the inhibitor efficiency increased with the inhibitor concentration and the testing temperature. Abbout et al. [15] used weight loss tests, potentiodynamic polarization curves and electrochemical impedance spectroscopy measurements and found that *Ceratonia siliqua* L. seed oil acts as a good corrosion inhibitor for iron in simulated acid rain with a maximum efficiency 98.6% at the highest inhibitor concentration, 750 ppm. On the other side, Pilić et al. [16] evaluated *Helichrysum italicum* leaves extract obtaining an efficiency of 50%. Varvara et al. [17] evaluated the ethanolic extract of *Aesculus hippocastanum* L. as a corrosion inhibitor of brass in acid rain, obtaining an efficiency of 94% with a concentration of 0.5 g/L. Rehioui et al. [18] studied the inhibitory effect of *Opuntia dillenii* seeds for

✉ J. G. Gonzalez-Rodriguez
ggonzalez@uaem.mx

¹ Centro de Investigacion en Ingenieria y Ciencias Aplicadas, Universidad Autonoma del Estado de Morelos, Av. Universidad 1001, Cuernavaca, MR, Mexico

² Facultad de Ciencias Quimicas e Ingenieria, Universidad Autonoma del Estado de Morelos, Av. Universidad 1001, Cuernavaca, MR, Mexico

iron in simulated acid rain obtaining an efficiency of 99% at a concentration of 750 ppm. Chraka et al. [19] evaluated essential oil and hydrosol extract of *Thymbra capitata* as green corrosion for brass in 3.5% NaCl. They found that in both cases, inhibitor efficiency increased with their concentration, but that for hydrosol extract was higher (93%) than that for essential oil (84%) and that the responsible compounds for that inhibition were carvacrol and eugenol contained in *T. capitata*. Fouda et al. [20] evaluated methanolic extract of *C. siliqua* as green corrosion inhibitor for copper and brass in nitric acid, finding that inhibitor efficiency increased with its concentration but decreased with testing temperature. Some corrosion inhibitors for bronze in alkaline media have been studied, as *Aloe vera* and *Robinia pseudoacacia* [21] obtaining efficiency values of 89% and 92%, respectively. Abdel-Karim [22] did an excellent review on the use of non-toxic inhibitors for protecting metals from acid rain corrosion, making special discussion in their adoption process. Some other researchers which evaluated green inhibitors using immersion tests in simulated acid rain solution are Tasić [23, 24], Rehioui [18] and Biswal [25]. All these research works have used immersion tests in a solution that tries to simulate an environment found in a corrosive atmosphere, finding suitable corrosion inhibitors whose mechanism is by adsorption, and although in a real atmosphere corrosion depends, among other factors, on wetting–drying cycles, temperature and humidity regimes or the presence of stronger oxidizing species and it is difficult to extrapolate the results to real conditions, these tests are as a first approach to find a suitable non-toxic corrosion inhibitor to try to reduce corrosion aggressiveness of a given atmosphere.

Thymus vulgaris is an aromatic plant which belongs to the Lamiaceae family, endemic from the Mediterranean region but it also grows in some other regions and is widely used for both culinary and medicinal [26–28]. Some research works have shown that *T. vulgaris* possess antioxidant, anti-inflammatory, anticoagulants, antibacterial and antifungal properties due to the presence of phenolic compounds present in thymol and carvacrol, which together with rosmarinic acid are some of the main compounds reported in *T. vulgaris* [29–34]. Thus, due to the presence of antioxidants within its internal structure, the goal of this research work is to evaluate the use of *T. vulgaris* L. extract as a green corrosion inhibitor for bronze in synthetic acid rain. For this purpose, both gravimetric and electrochemical tests will be used.

2 Experimental Procedure

2.1 Testing Material

Employed testing material includes commercial bar bronze 10 mm in diameter with chemical composition as given in Table 1. This table shows that the main chemical elements of this alloy are Cu, Sn and Zn, with more than 97% of the total contents of the alloy, followed by 1.93% Al.

2.2 Inhibitor Synthesis

Thymus vulgaris leaves (60 g), which were obtained in a local market, were ground and soaked in methanol (120 ml) at room temperature for 14 days. After this, the solution was filtered and the methanol was allowed to evaporate at room temperature obtaining a green, sticky extract which was added in to the working electrolyte at different concentrations including 0, 100, 200, 400, 600, 800 and 1000 ppm. The extract was analysed by using the fast Fourier infrared spectroscopy (FTIR) technique by using a Bruker equipment in KBr pellet in the 4000–470 cm^{-1} interval. To detect the majority of organic natural compounds contained in the methanol extract, a Gas Chromatography Agilent 6890 System Plus coupled to Agilent 5973 Network Mass selective detector.

2.3 Testing Solution

As a working electrolyte, a simulated acid rain containing Sulphuric acid (0.06 ml/L), Nitric acid (0.02 ml/L), Sodium nitrate (0.0265 g/L), Ammonium sulphate (0.0462 g/L), Sodium sulphate (0.0345 g/L), and Sodium chloride (0.0875 g/L) was used. Deionized water was used for this purpose, whereas all reactants were analytical grade from Sigma-Aldrich.

2.4 Gravimetric Tests

For weight loss experiments, cylindrical specimens measuring 10 mm in diameter and 3 mm in thickness were used. They were polished up to 600 grade SiC emerging paper, washed with water, rinsed with acetone and dried with hot air. Tests were carried out at different inhibitor concentrations at room temperature, close to 25 °C. 40 and 60 °C during 72 h. Three specimens were used for each inhibitor concentration. Before starting the experiments, the total area and initial weight for each one of the specimens were measured. After the experiments, corrosion products were removed from the specimens

Table 1 Chemical composition of testing bronze, wt%

Element	Cu	Sn	Zn	Ni	Pb	Fe	Al
%	85.06	7.83	4.23	1.93	0.80	0.10	0.06

and the final weight was measured. Metal weight loss, ΔW , was calculated according to [35]:

$$\Delta W = (M_i - M_f) / (M_f * A_i * T) \quad (1)$$

where M_i and M_f are the specimen's initial and final mass, A_i the initial exposed area, and T is the total exposure time, 72 h. Inhibitor efficiency, IE was calculated using the following expression [35]:

$$IE = (\Delta W_b - \Delta W_{inh}) / \Delta W_b \times 100 \quad (2)$$

where ΔW_b is the weight loss for the blank, uninhibited solution, and ΔW_{inh} the weight loss for the inhibitor-containing solution, respectively. Inhibitor efficiency data were used to calculate the metal surface area covered by the inhibitor, θ , according to:

$$\theta = IE / 100 \quad (3)$$

Selected specimens were observed in a low vacuum LEO Scanning electronic microscope (SEM) whereas micro-chemical analysis was carried out using an energy-dispersive X-ray analyser (EDX) attached to it.

2.5 Electrochemical Techniques

Electrochemical techniques used included potentiodynamic polarization curves and electrochemical impedance spectroscopy. The open circuit potential value (OCP) was monitored during the whole experiment as well. An electrochemical cell containing the bronze specimen as working electrode, a 6.00 mm graphite rod as counter electrode and a silver/silver chloride reference electrode was utilized. Specimens measuring 10 mm in diameter and 3 mm in thickness were spot welded to a copper wire and encapsulated in commercial polymeric resin. Potentiodynamic polarization curves were started by cathodically polarizing the specimen 1000 mV more cathodic than the free corrosion potential value, E_{corr} , and scanned towards the anodic direction at a

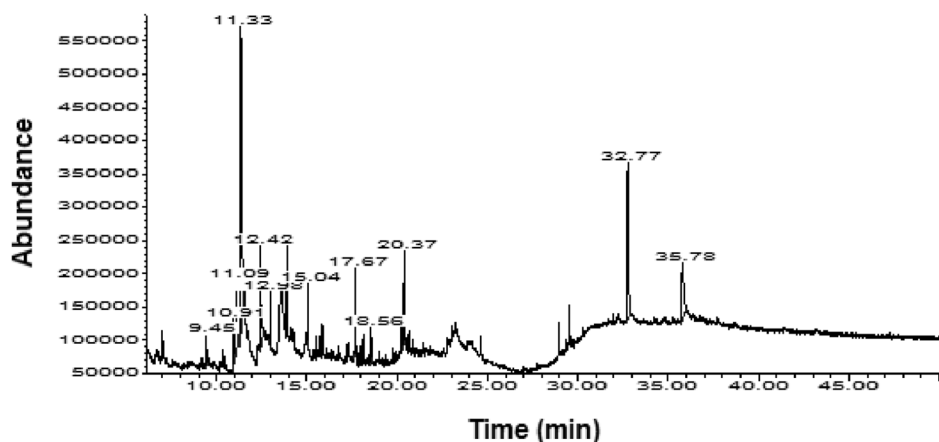
scan rate of 1 mV/s and ending at a potential value 1000 mV more anodic than E_{corr} . Corrosion current density value, I_{corr} was calculated using Tafel extrapolation. Electrochemical impedance spectroscopy experiments (EIS) were performed by applying an AC signal ± 15 mV peak-to-peak at the E_{corr} value in a frequency interval 0.01–100,000 Hz. A Gamry potentiostat was used for these experiments.

3 Results and Discussion

3.1 Inhibitor Characterization

Chromatogram of the *T. vulgaris* extract is given in Fig. 1 which shows a peak at a retention time of 9.45 min and corresponds to borneol; phenol was detected at retention times of 10.91, 11.09 and 11.33 min. 2-metil-5-(1-metilethyl) was detected at a retention time of 12.42 min, whereas the peak shown at 12.98 min corresponds to 1,4-benzenediol. Caryophyllene was found at a retention time of 15.04 min, caryophyllene oxide at 17.67 min, Tetramethyl-2-hexadecen-1-ol at 3, 7, 11 and 15 min. The peak detected at 18.56 min corresponds to the dexamecanoic acid, phytol at 20.37 min, D, α -tocopherol (vitamin E) at a retention time of 32.77 min and β -Sitosterol was detected at a retention time of 35.78 min. The most abundant compounds were phenol, 2-metil-5-(1-metilethyl)- and D, α -tocopherol, therefore, it can be said that phenolic compounds are present in the methanolic extract of *T. vulgaris*, all of them containing C within their chemical structure, which provides to this extract antioxidant properties. In fact, α -tocopherol has been reported as a corrosion inhibitor also for Cu and a Cu–40Zn alloys in acid rain, having an efficiency value of 90% [36]. The inhibitory properties of these components is due to the presence of functional groups such as O–H, C–H, C=C and C–O among others as reported by other researchers [37, 38]. In both works, the authors declare that the inhibitory characteristics of the extracts they used as green corrosion

Fig. 1 Chromatogram of methanolic *T. vulgaris* extract



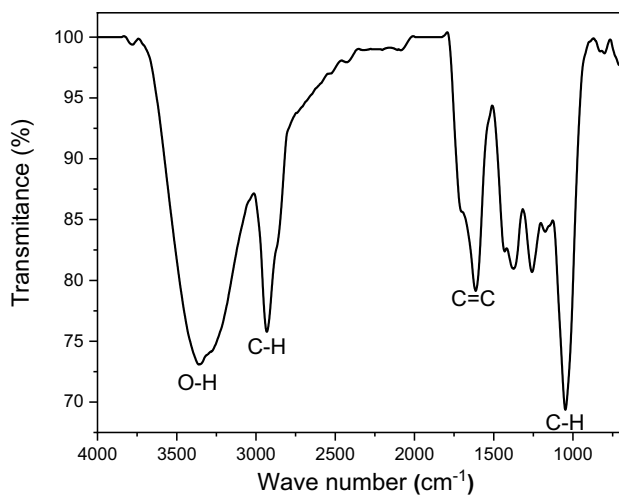


Fig. 2 FTIR diagram of methanolic *T. vulgaris* extract

inhibitors, *Spirogyra algae* and *Brassica oleracea* was due to the presence of hydroxyl, amino and carboxyl groups in the extracts. In fact, some of these functional groups were detected in the *T. vulgaris* extract, as shown in the FTIR diagram shown in Fig. 2, which shows the presence of the hydroxyl group (O–H), in a wide interval between 3436 and 3206 cm^{-1} , at 2927 cm^{-1} the C–H group is detected, at 1615 cm^{-1} appears the presence of the C=C group, whereas at 1047 cm^{-1} the C–O group is present. The presence of heteroatoms such C and O directly attached to the aromatic ring enhances the availability of π -electrons to get bonded to the vacant d-orbital of Cu.

3.2 Gravimetric Tests

The effect of *T. vulgaris* concentration and testing temperature on the weight loss, inhibitor efficiency and metal surface area covered by the inhibitor for bronze in synthetic acid rain is shown in Table 2. This table shows that, at a fixed temperature, the metal weight loss decreases with an increase in the *T. vulgaris* concentration up to a concentration of 800 ppm, and a further increase in its concentration brings an increase in the alloy weight loss. In a similar way, inhibitor efficiency increases with increasing its concentration up to an inhibitor concentration of 800 ppm, obtaining a value of 90.1%, decreasing with a further increase in the *T. vulgaris* concentration. The decrease in the weight loss and the increase in its inhibitor efficiency with the inhibitor concentration is due to its adsorption on the metal surface as indicated by the increase on the metal surface area covered by the inhibitor, θ , which increases with the inhibitor concentration up to an inhibitor concentration and it decreases with a further increase in the *T. vulgaris* concentration. As the testing temperature increases, the metal weight loss

Table 2 Effect of *T. Vulgaris* concentration and testing temperature on the weight loss, inhibitor efficiency and metal surface area covered by the inhibitor for brass in synthetic acid rain

Temp. ($^{\circ}\text{C}$)	C_{inh} (ppm)	ΔW ($\text{mg}/\text{cm}^2 \text{ h}$)	I.E. (%)	θ
25	0	0.86	–	–
	100	0.47	46.2	0.46
	200	0.37	78.3	0.78
	400	0.20	83.6	0.83
	600	0.12	87.9	0.88
	800	0.086	90.1	0.90
40	1000	0.20	84.0	0.84
	0	4.8	–	–
	100	2.6	42.5	0.42
	200	1.0	69.3	0.69
	400	0.82	73.1	0.73
	600	0.67	78.1	0.78
60	800	0.33	85.1	0.85
	1000	0.53	81.1	0.81
	0	11.8	–	–
	100	7.1	35.3	0.35
	200	5.3	58.1	0.58
	400	4.2	63.3	0.63
	600	3.5	69.6	0.69
	800	1.56	78.3	0.78
	1000	2.68	71.7	0.72

increases and the inhibitor efficiency decreases, but at the different testing temperatures, the maximum efficiency was reached at an *T. vulgaris* concentration of 800 ppm, reaching values of 85.1 and 78.3 at 40 and 60 $^{\circ}\text{C}$, respectively. Benzidia et al. [21] obtained similar results with the use of *A. vera* with a Cu- 5–21 Sn with less than 1% Zn in 3% NaCl solution, using only 50, 100 and 150 ppm of inhibitor, and reaching its maximum efficiency of 98% with 150 ppm.

To get more information on the way that *T. vulgaris* extract is adsorbed on to the metal surface area, different adsorption isotherms were used and, as it can be seen in Fig. 3, Langmuir type of adsorption isotherm gave the best fit [39] which relates the metal surface area covered by the inhibitor and its concentration, C_{inh} , according to following expression [39]:

$$\frac{C_{\text{inh}}}{\theta} = \frac{1}{K_{\text{ads}}} + C_{\text{inh}} \quad (4)$$

where K_{ads} is the adsorption constant and can be calculated by using [40]:

$$\Delta G_{\text{ads}}^0 = -RT \ln(10^6 K_{\text{ads}}) \quad (5)$$

where ΔG_{ads}^0 is the standard free energy, R the universal gas constant, and T is the absolute temperature. According to

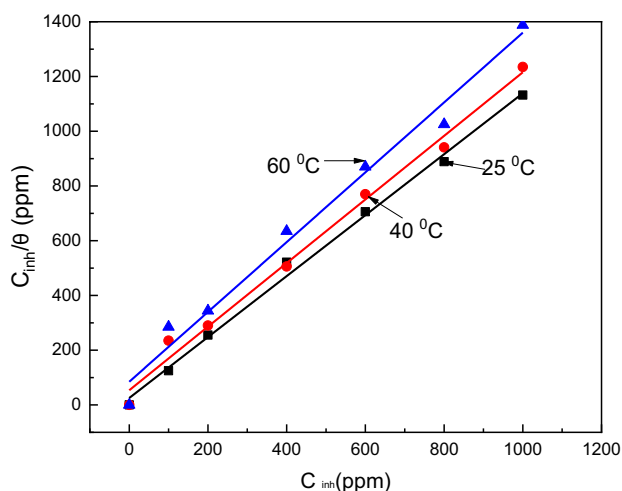


Fig. 3 Langmuir type of adsorption isotherm for *T. vulgaris* extract

[40] for values of ΔG_{ads}^0 around or less negative than -20 kJ/mol, the relation between inhibitor and metal surface is physical-type, ie, electrostatic attraction. From data given in Fig. 1 and knowing that according to Eq. (4) the intercepts of the straight line is $\frac{1}{K_{ads}}$, the obtained values for ΔG_{ads}^0 were -23.52 , -19.42 and -15.71 kJ/mol at 25, 40 and 60 °C respectively, indicating a mixed physical and chemical adsorption mechanism dominated by a weak, physical mechanism.

From data given in Table 2 it can be seen that the metal weight loss increases as the temperature increases, and the relationship between weight loss and the testing temperature is given by Arrhenius equation given by [41]:

$$\Delta W = Ae\left(\frac{-E_a}{RT}\right) \tag{6}$$

where A is the Arrhenius pre-exponential factor, E_a the apparent activation energy (J/mol), R the gases universal constant ($8.314 \text{ J mol}^{-1} \text{ K}^{-1}$), and T the absolute temperature (K). By plotting $\log(\Delta m)$ versus $1/T$, as given in Fig. 4, the apparent activation energy values for each inhibitor concentration can be calculated as shown by data given in Table 3. This table shows that the apparent activation energy values increase in presence of *T. vulgaris* extract and with its concentration up to an inhibitor concentration of 800 ppm, but it decreases again at 1000 ppm. The increase in the apparent activation energy values indicates that the corrosion process is more difficult in presence of *T. vulgaris*; the highest values

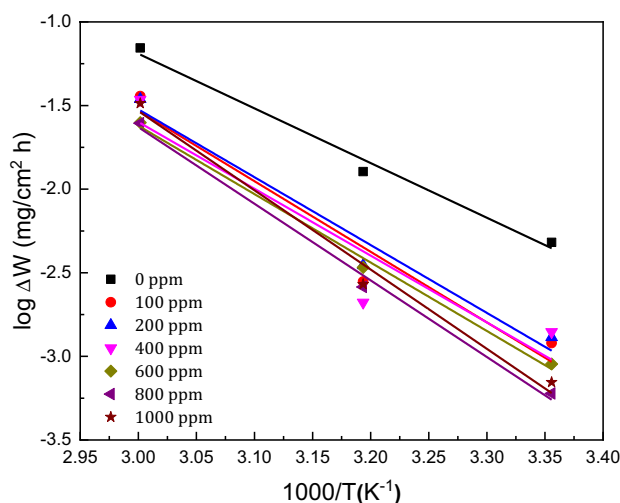


Fig. 4 Arrhenius plots for the weight loss of bronze in synthetic acid rain containing different concentrations of *T. vulgaris* extract

were obtained at 800 ppm, where the highest *T. Vulgaris* efficiency values were obtained [42].

3.3 Electrochemical Tests

The effect of *T. vulgaris* concentration on the OCP value for bronze in simulated acid rain is shown in Fig. 5. For the solution in absence of inhibitor, the OCP value was the noblest during the first 6 h of testing and remained more or less constant around a value of -25 mV. With the addition of *T. vulgaris*, the OCP value reached values between -225 and -125 mV, but it rapidly shifted towards nobler values regardless the inhibitor concentration, reaching a steady state after a period that fluctuated between 6 and 10 h depending on the *T. vulgaris* concentration. This shift in to the noble direction is due to the adsorption of *T. Vulgaris* and to the formation of a protective layer of corrosion products. After 10 h of testing, the noblest OCP value was reached with the addition of 800 and 1000 ppm, precisely where the highest inhibitor efficiency values were obtained. Lower inhibitor than 800 ppm induced more active OCP values than that obtained in the uninhibited solution, indicating that there was not a clear trend on the OCP value with the inhibitor concentration.

Potentiodynamic polarization curves for bronze in synthetic acid rain containing different amounts of *T. Vulgaris* are shown in Fig. 6, whereas electrochemical parameters such as E_{corr} , I_{corr} , anodic and cathodic Tafel slopes, β_a and β_c , respectively, together with inhibitor efficiency, are shown in Table 4. In this case, inhibitor efficiency values were calculated using following expression [35]:

Table 3 Effect of the *T. vulgaris* concentration on the apparent activation energy values for bronze in simulated acid rain at 25 °C

C_{inh} (ppm)	0	100	200	400	600	800	1000
E_a (J/mol)	27.2	32.1	33.2	33.7	34.0	39.4	38.0

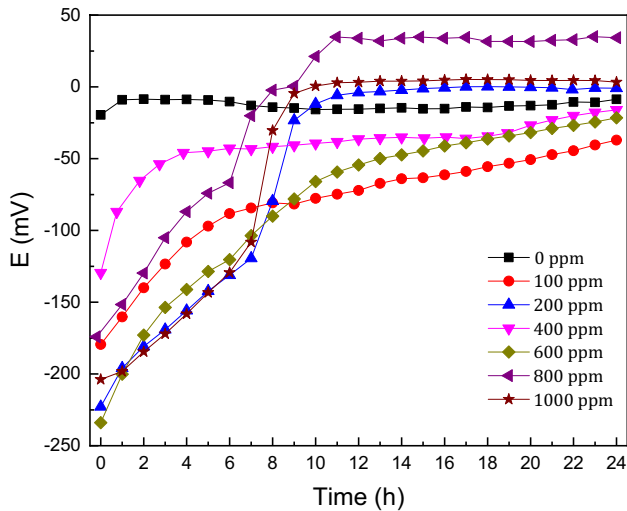


Fig. 5 Effect of the *T. vulgaris* extract on the OCP value for bronze in synthetic acid rain

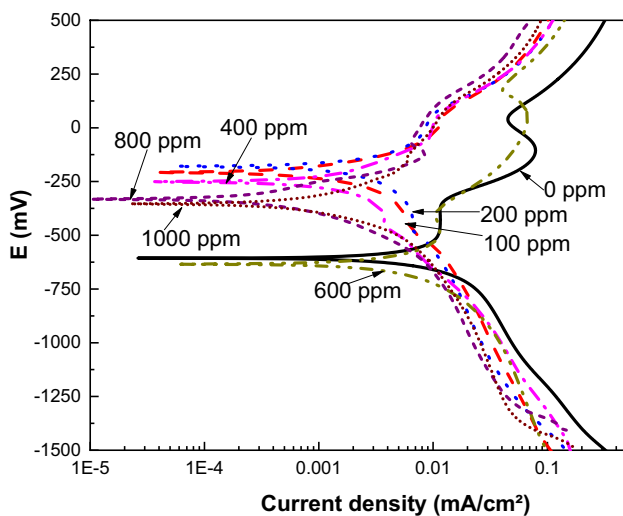


Fig. 6 Effect of the *T. vulgaris* extract on the polarization curves for bronze in synthetic acid rain

$$IE = (I_{corr1} - I_{corr2}) / I_{corr1} \times 100 \tag{7}$$

where I_{corr1} and I_{corr2} are the corrosion current density values without and with inhibitor, respectively. In absence of *T. vulgaris*, data display an active–passive behavior with two passive regions in the anodic branch of the curve, the first

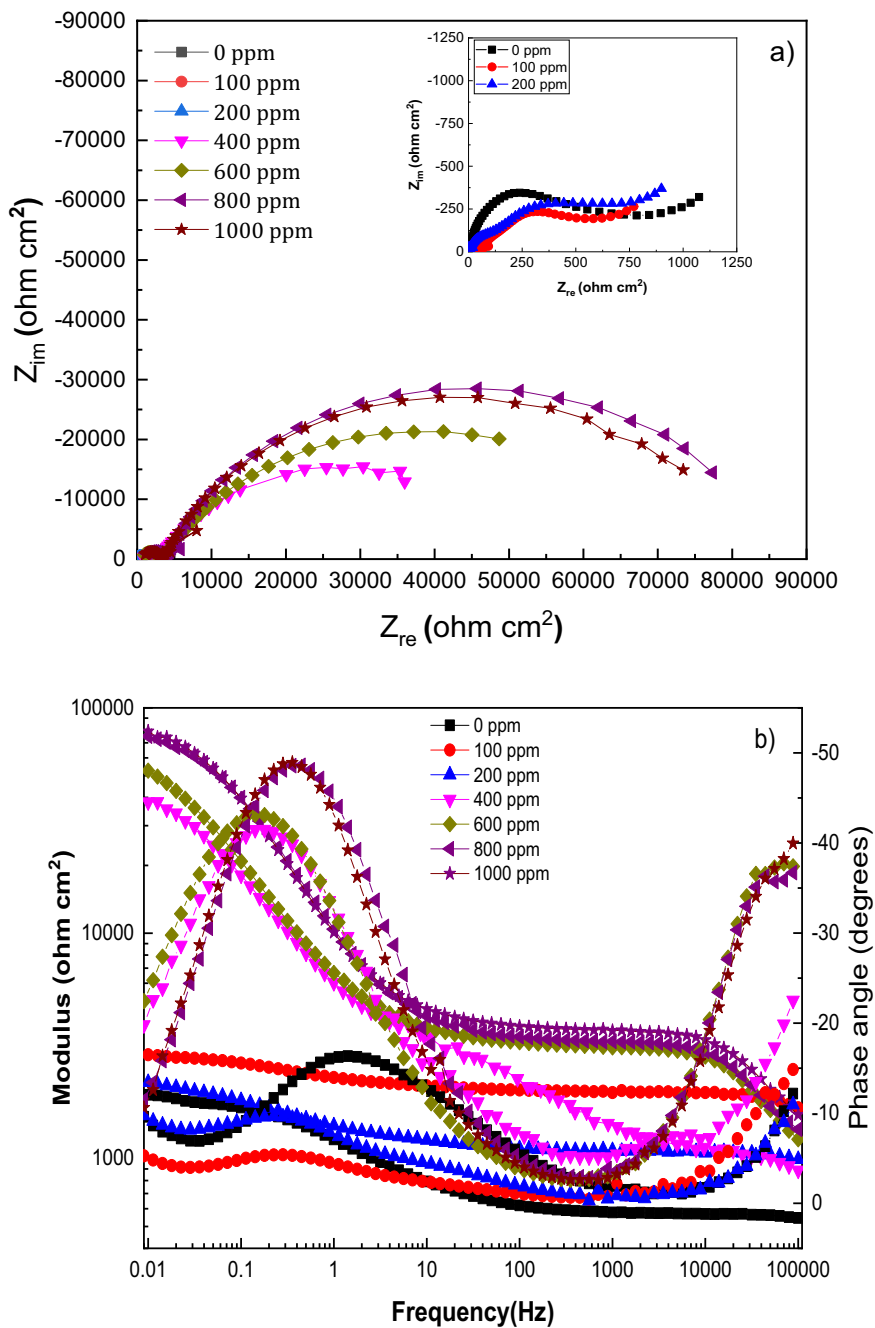
zone starts at a potential value of -500 mV and finishes at a pitting potential value close to -340 mV, and a second region between 15 and 55 mV. On the cathodic branch of the curve the increase in the current density is due to the oxygen reduction reaction. It is evident from curves displayed in Fig. 6 that the addition of different concentrations of *T. vulgaris* decreases both the anodic and cathodic current density values, indicating that this extract affects both bronze anodic dissolution and oxygen reduction reactions by forming protective corrosion products layers, since the passive zone is shown even in presence of the inhibitor. The addition of *T. vulgaris* decreased the I_{corr} value in absence of inhibitor from 0.016 down to 0.0004 mA/cm², the lowest value obtained with the addition of 800 ppm of inhibitor, a decrease in almost two orders of magnitude, and an inhibitor efficiency value of 97.5%, as shown in Table 4, which decreased with a further increase in the inhibitor concentration of 1000 ppm, similar to the gravimetric results. Similar results were obtained with the use of Sulfamethoxazole [19, 20]. There was not a clear trend of the E_{corr} value with the addition of *T. vulgaris*, since for all the inhibitor concentrations except 600 ppm, this parameter shifted towards nobler values, whereas with the addition of 600 ppm of inhibitor, the E_{corr} value became more active than the value obtained in absence of *T. vulgaris*. However, anodic Tafel slope was increased whereas the cathodic Tafel slope was decreased with the addition of *T. vulgaris*, thus having a more pronounced effect on the anodic bronze dissolution than in the cathodic hydrogen evolution reactions, behaving thus as an anodic type of inhibitor. The metal surface area covered by *T. vulgaris* increased with an increase in the inhibitor up to a value of 800 ppm and decreases when this concentration increases further to 1000 ppm due to the inhibitor desorption from the metal surface. These findings are consistent with the formation of protective corrosion products layer by the *T. vulgaris* compounds which are able to be adsorbed onto the bronze surface and slow down both anodic dissolution and cathodic hydrogen evolution reactions with a higher effect on the anodic one.

EIS data in both Nyquist and Bode formats for bronze in simulated acid rain containing different concentrations of *T. vulgaris* are given in Fig. 7. Nyquist data for inhibitor concentration lower than 200 ppm, Fig. 7a insert, describe a depressed, capacitive semicircle at high and intermediate frequency values followed by what looks like a second, unfinished semicircle. Such a behaviour has been reported

Table 4 Electrochemical parameters obtained from polarization curves for bronze in synthetic acid rain in presence of *T. Vulgaris*

C_{inh} (ppm)	E_{corr} (mV)	I_{corr} (mA/cm ²)	β_a (mV/dec)	β_c (mV/dec)	IE (%)	θ
0	-595	0.016	125	415	-	-
100	-215	0.005	180	400	68	0.68
200	-180	0.004	200	375	75	0.75
400	-250	0.002	220	260	87.5	0.87
600	-635	0.001	250	345	93.7	0.94
800	-325	0.0004	180	260	97.5	0.98
1000	-350	0.0008	260	250	95	0.95

Fig. 7 **a** Nyquist and **b** bode plots for bronze in synthetic acid rain containing different concentrations of *T. vulgaris* extract



for Copper and its alloys in acidic solutions, as for instance by Tasić et al. [23], when using Ibuprofen a corrosion inhibitor for Copper in synthetic acid rain. The presence of the low-frequency semicircle was much clearer for inhibitor concentrations higher than 200 ppm, where Nyquist diagrams describe a depressed semicircle at high and intermediate frequency values, followed by a second semicircle at lower frequency values, indicating a charge-transfer controlled corrosion process. The semicircle diameter increases with the *T. vulgaris* concentration, reaching its highest value at a concentration of 800 ppm, decreasing with a further increase in the inhibitor concentration of 1000 ppm. The high and intermediate frequency semicircle is related with the electrochemical reactions taking place at the metal/double electrochemical layer interface, whereas the low-frequency loop is related to the redox processes taking place at the metal/corrosion products layer interface [18–20, 41]. Bode diagrams in the Modulus format, Fig. 7b, show an increase in the impedance modulus as the *T. vulgaris* concentration increases, reaching its highest value at a concentration of 800 ppm due to the bronze corrosion inhibition by the inhibitor. Additionally, phase angle plots show an increase in this value in presence of the inhibitor than in its absence, which implies the metal dissolution inhibition by the *T. Vulgaris* compounds.

Experimental EIS results were fitted with the use of equivalent electric circuits shown in Fig. 8. In these circuits, R_s represents the electrolyte resistance, R_{ct} the charge transfer resistance, C_{dl} and C_f are the double electrochemical layer and corrosion products film capacitances, respectively. Due to surface heterogeneities due to surface imperfections,

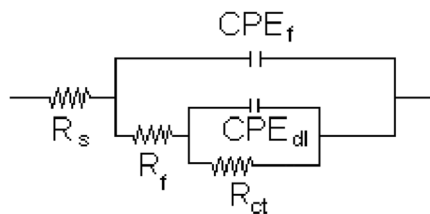


Fig. 8 Electric circuit used to simulate EIS data

Table 5 Electrochemical parameters obtained from fitting EIS data

C_{inh} (ppm)	CPE_{dl} (F/cm ²)	n_{dl}	R_{dl} (ohm cm ²)	CPE_f (F/cm ²)	n_f	R_f (ohm cm ²)	IE (%)
0	5.8×10^{-4}	0.6	623	8.1×10^{-4}	0.5	790	–
100	1.3×10^{-4}	0.6	768	5.3×10^{-4}	0.6	1090	27
200	7.9×10^{-5}	0.6	916	1.1×10^{-4}	0.7	1125	30
400	6.7×10^{-6}	0.7	1656	6.4×10^{-5}	0.7	23,912	88
600	1.3×10^{-8}	0.8	2749	5.2×10^{-5}	0.8	32,790	91
800	1.5×10^{-8}	0.8	2907	3.7×10^{-5}	0.9	51,640	98
1000	1.5×10^{-8}	0.8	3425	2.9×10^{-5}	0.8	48,785	94

roughness due to metal dissolution, ideal capacitances such as C_{dl} and C_f are replaced by constant phase elements, CPE, whose impedance is calculated by:

$$Z_{CPE} = 1/[C(i\omega)n] \quad (8)$$

where $i = -1^{1/2}$, ω the angular frequency and n is a physical parameter that gives interphase properties of the working electrode such as roughness, inhibitor adsorption, etc. The resulting parameters from the use of circuits given in Fig. 8 for tests at different temperatures are shown in Table 5. This table clearly shows that the R_{ct} values are much lower than those for R_f , and, thus, the corrosion products film resistance is responsible for the corrosion resistance of the alloy. Value for R_f increases with an increase in the *T. vulgaris* concentration, reaching its highest value at an inhibitor concentration of 800 ppm, and then it decreases at 1000 ppm, similar to the behaviour observed in gravimetric tests and in the I_{corr} values. Values for R_f , R_{ct} , CPE_f and CPE_{dl} are typical of copper and its alloys in simulated acid rain solutions [18, 19, 40]. Conversely to the R_{ct} behaviour, CPE_{dl} values decreased with an increase in the inhibitor concentration due to the fact that *T. vulgaris* molecules, which have lower dielectric constant, ϵ , than that for water molecules that are replaced by the inhibitor molecules [43, 44]. Relationship between double electrochemical layer capacitance, C_{dl} , dielectric constant and double layer thickness, δ , is given by:

$$C_{dl} = \epsilon\epsilon_0 A/\delta \quad (9)$$

where ϵ_0 is the vacuum electrical permittivity, and A the surface area. Thus, if the dielectric constant decreases or the thickness of the double-layer increases, the capacitance value decreases. In this case, inhibitor efficiency values, IE , were calculated by using the following equation:

$$IE = \frac{R_{p/inh} - R_p}{R_{p/inh}} \times 100 \quad (10)$$

where R_p and $R_{p/inh}$ are the polarization resistance without and with inhibitor, which is the sum of $R_s + R_f + R_{ct}$, the resistance values across the metal/double electrochemical

layer/corrosion products film interfaces. Similar values for R_p and R_{ct} have been reported for copper and its alloys in synthetic acid rain solutions [18–20]. It can be seen from data shown in Table 5 that inhibitor efficiency increases with its concentration obtaining a maximum value of 98% with an inhibitor concentration of 800 ppm. An increase in the *T. vulgaris* concentration up to 1000 ppm brings a decrease in the inhibitor efficiency value as given by the weight loss and polarization curves results above.

3.4 Corroded Surfaces Characterization

SEM micrographs of corroded bronze specimens in simulated acid rain solution in absence and presence of 800 ppm of *T. vulgaris* are shown in Fig. 9 whereas the chemical composition of the corrosion products is given in Fig. 10. Specimen corroded in the uninhibited solution, Fig. 9a, exhibits a surface metal without the formation of a complete corrosion product film together with some localized type of corrosion such as pits. EDX microchemical composition of the corrosion product film, Fig. 10a and Table 6, shows the presence of chemical elements either from the alloy, such as Cu, O, Zn, Pb, S and Al. On the other hand, specimen corroded in

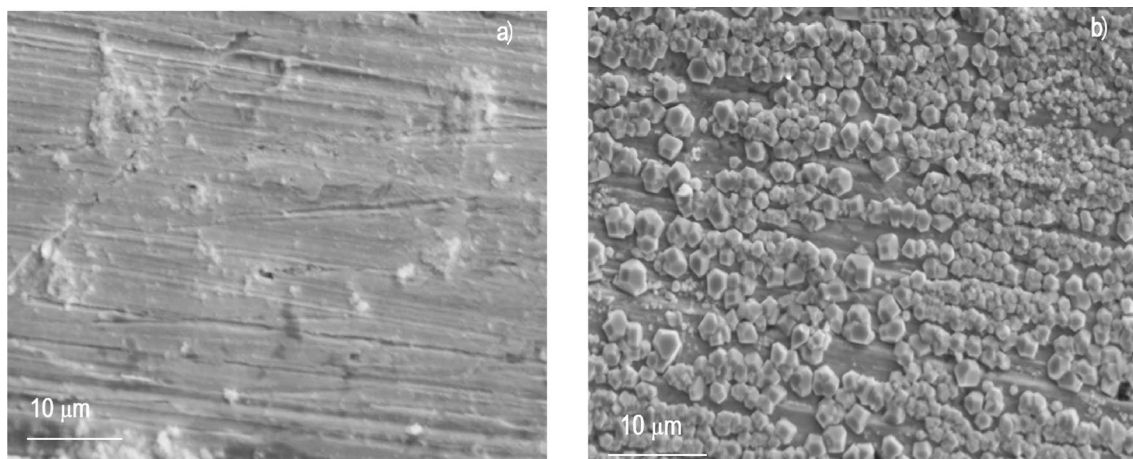


Fig. 9 SEM micrographs of specimens corroded in synthetic acid rain solution containing a 0 and b 800 ppm of *T. vulgaris* extract

Fig. 10 EDX micro chemical analysis of corrosion products found on specimens corroded in synthetic acid rain solution containing a 0 and b 800 ppm of *T. vulgaris* extract

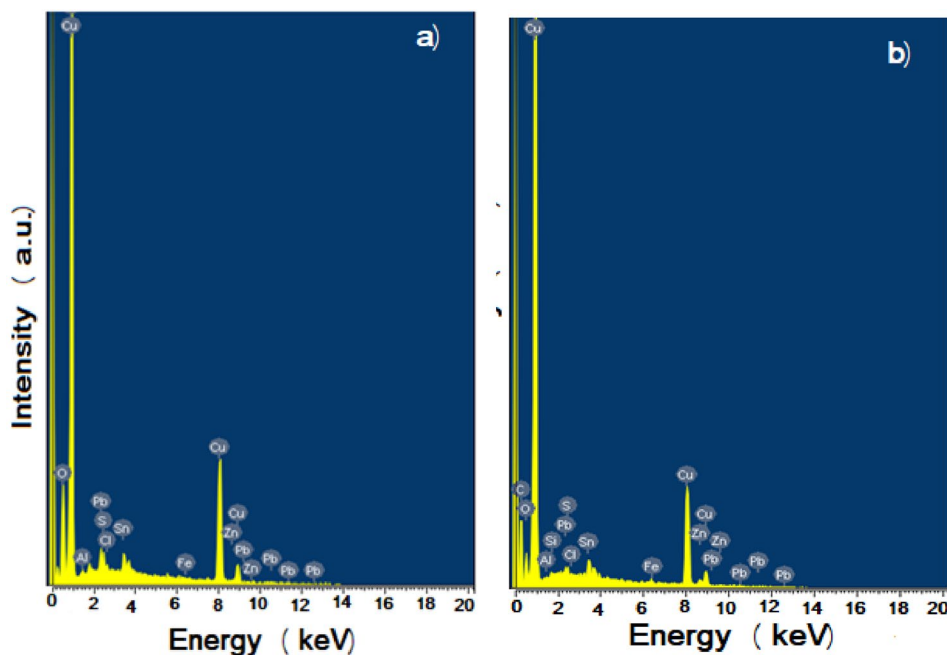


Table 6 Quantitative results of the corrosion products layer analysis for specimens corroded at 25 °C in absence and presence of 800 ppm of *Thymus vulgaris*

Element	wt%	
	0 ppm	800 ppm
O	12.04	3.90
C	–	20.58
Na	0.18	1.17
Al	0.13	0.04
S	0.43	0.04
Cl	0.47	0.12
Fe	0.18	0.83
Cu	76.49	63.98
Zn	1.80	3.40
Sn	0.59	4.55
Pb	3.57	1.18

presence of 800 ppm of *T. vulgaris*, Fig. 9b and Table 6, shows the presence of a more compact, more uniform layer of corrosion products film, with some uncovered parts of the metal by this film, indicating why the inhibitor efficiency values were lower than 100%. Chemical composition of this layer, Fig. 10b, shows the same chemical elements found in specimen corroded in the uninhibited solution, i.e., Cu, O, Zn, Pb, S and Al in addition to the presence of C, which comes from an organic compound such as those contained in *T. vulgaris*. For specimen corroded in the uninhibited solution, main chemical elements were Cu and O, indicating the formation of a copper oxide, responsible for the passive layer found in the polarization curves, Fig. 6, that gives some corrosion protection under these conditions. On the other hand, corrosion products found on specimen corroded in presence of 800 ppm of *T. vulgaris*, the presence of C indicates that compounds found in the extract are adsorbed on to the metal surface, since all of them contain C within their chemical structure. The contents of O and Cu are lower than that found for specimen corroded in absence of inhibitor, due to the adsorption of extract rather than formation passive film. In addition to this, the Zn and Sn in the corrosion products film corroded in presence of inhibitor is higher than that for metal corroded in its absence. Some metals decrease because of their dissolution and others increase due to form metal–extract complexes.

4 Conclusions

1. The goal of using extract of *T. vulgaris* leaves as corrosion inhibitor for bronze in simulated acid rain solution was certainly achieved, since it was found to be a good inhibitor with an efficiency that increases with the inhibitor concentration up to 800 ppm, reaching values higher than 90%, and decreases with a further increase inhibitor concentration and with the testing temperature.

2. *Thymus vulgaris* extract behaved as an anodic type of inhibitor, affecting the anodic bronze dissolution more than the cathodic hydrogen evolution reactions.
3. Extract formed a layer of corrosion products film due to its adsorption on to the metal surface following a Langmuir type of adsorption isotherm in a physical–chemical mixed type of adsorption mechanism dominated by the weak, physical type of adsorption.
4. Main compounds detected in the extract included phenol, 2-metil-5-(1-metilethyl)- and D, α -tocopherol, which provide inhibitory properties to the extract due to the presence of heteroatoms, mainly C and O, within its chemical structure.

Author Contributions All authors contributed to the study conception and design. Material preparation, data collection and analysis were performed by DGG-G, AKL-G and RL-S. The first draft of the manuscript was written by JGG-R and all authors commented on previous versions of the manuscript. All authors read and approved the final manuscript.

Funding The authors declare that no funds, grants, or other support were received during the preparation of this manuscript.

Data Availability Data will be available on reasonable request.

Declarations

Conflict of interest The authors have no relevant financial or non-financial interests to disclose.

References

1. Chang T, Herting G, Goidanich S, Sánchez Amaya JM, Arenas MA, Le Bozec N, Leygra I, Odnevall Wallinder I (2019) The role of Sn on the long-term atmospheric corrosion of binary Cu-Sn bronze alloys in architecture. *Corros Sci* 149:54–67. <https://doi.org/10.1016/j.corsci.2019.01.002>
2. Liang Z, Jiang K, Zhang T, Dou Z (2019) Corrosion behavior of Cu–Sn bronze alloys in simulated archeological soil media. *Mater Corros* 71:617–627. <https://doi.org/10.1002/maco.201911338>
3. Petiti C, Toniolo L, Gulotta D, Mariani B, Goidanich S (2020) Effects of cleaning procedures on the long-term corrosion behavior of bronze artifacts of the cultural heritage in outdoor environment. *Environ Sci Pollut Res* 27:3081–13094. <https://doi.org/10.1007/s11356-020-07814-4>
4. Chang T, Maltseva A, Volovitch P, Odnevall Wallinder I, Leygraf C (2020) A mechanistic study of stratified patina evolution on Sn-bronze in chloride-rich atmospheres. *Corros Sci* 166:108477. <https://doi.org/10.1016/j.corsci.2020.108477>
5. Liu Z, Yang J, Zhang J, Xiang H, Wei H (2019) A bibliometric analysis of research on acid rain. *Sustainability* 11:3077–3084. <https://doi.org/10.3390/su11113077>
6. Szilvia S, Nagy M, Juhász L, Bubonyi T, Péter B, Forgács G, Bakonyi E (2020) Conservation purpose material testing of corrosion products on outdoor bronze statues. *IOP Conf Ser: Mater Sci Eng* 903:012037–012044. <https://doi.org/10.1088/1757-899X/903/1/012037>

7. Letardi P (2021) Testing new coatings for outdoor bronze monuments: a methodological overview. *Coatings* 11:131–140. <https://doi.org/10.3390/coatings11020131>
8. Abdel-Karim AM, El-Shamy AM (2022) A review on green corrosion inhibitors for protection of archeological metal artifacts. *J Bio Tribo Corros*. <https://doi.org/10.1007/s40735-022-00636-6>
9. Marzorati S, Verotta L, Trasatti SP (2019) Green corrosion inhibitors from natural sources and biomass wastes. *Molecules* 24:48–57. <https://doi.org/10.3390/molecules24010048>
10. Miralrio A, Espinoza Vázquez A (2020) Plant extracts as green corrosion inhibitors for different metal surfaces and corrosive media: a review. *Processes* 8:942–953. <https://doi.org/10.3390/pr8080942>
11. Popoola LT (2020) Progress on pharmaceutical drugs, plant extracts and ionic liquids as corrosion inhibitors. *Heliyon* 5:01143–01152. <https://doi.org/10.1016/j.heliyon.2019.e01143>
12. Singh CD, Verma C, Quraishi MA (2021) Molecular structural aspects of organic corrosion inhibitors: experimental and computational insights. *J Mol Struct* 1227:129374. <https://doi.org/10.1016/j.molstruc.2020.129374>
13. Sharma S, Kumar A (2021) Recent advances in metallic corrosion inhibition: a review. *J Mol Liq* 322:114862. <https://doi.org/10.1016/j.molliq.2020.114862>
14. Binyehmed FM, Abdullah AM, Zainal Z, Zawawi RM (2018) Green coffee bean extract as a green corrosion inhibitor for aluminium in artificial acid rain medium. *Int J Appl Environ* 13:171–183
15. About S, Chellouli M, Zouarhi M, Benzidia B, Hammouch H, Chebabe D, Dermaj A, Erramli H, Bettach N, Hajjaji N (2018) New formulation based on *Ceratonia siliqua* L. Seed oil, as a green corrosion inhibitor of iron in acidic medium. *Anal Bioanal Electrochem* 10:789–804
16. Pilić Z, Martinović I (2019) Effect of *Helichrysum italicum* on the corrosion of copper in simulated acid rain solution. *Chem Biochem Eng Q* 33:449–457. <https://doi.org/10.15255/CABEQ.2019.1614>
17. Varvara S, Caniglia G, Izquierdo J, Bostan R, Găină L, Bobis O, Souto RM (2020) Multiscale electrochemical analysis of the corrosion control of bronze in simulated acid rain by horsechestnut (*Aesculus hippocastanum* L.) extract as green inhibitor. *Corros Sci* 165:108381. <https://doi.org/10.1016/j.corsci.2019.108381>
18. Rehioui M, About S, Benzidia B, Hammouch H, Erramli H, Daoud NA, Badrane N, Hajjaji N (2021) Corrosion inhibiting effect of a green formulation based on *Opuntia dillenii* seed oil for iron in acid rain solution. *Heliyon* 7:06674–06682. <https://doi.org/10.1016/j.heliyon.2021.e06674>
19. Chraka A, Raissouni I, Ben SN, Khayar S, Mansour A, Tazi S, Chaouket F, Bouchta D (2020) Identification of potential green inhibitors extracted from *Thymbra capitata* (L.) Cav. for the corrosion of Brass in 3% NaCl solution: experimental, SEM–EDX analysis, DFT computation and Monte Carlo simulation studies. *J Bio Tribo Corros* 6:80–99. <https://doi.org/10.1007/s40735-020-00377-4>
20. Fouda AS, Shalabi K, Idress AA (2015) *Ceratonia siliqua* extract as a green corrosion inhibitor for copper and brass in nitric acid solutions. *Green Chem Lett Rev* 8:17–29. <https://doi.org/10.1080/17518253.2015.1073797>
21. Benzidia B, Hammouch H, Dermaj A, Benassaoui H, About S, Hajjaji N (2019) Investigation of green corrosion inhibitor based on *Aloe vera* (L.) Burm. F. for the protection of bronze B66 in 3% NaCl. *Anal Bioanal Electrochem* 11:165–177
22. Abdel-Karim AM, El-Shamy AM (2022) A review on green corrosion inhibitors for protection of archeological metal artifacts. *J Bio Tribo Corros* 8:35–43. <https://doi.org/10.1007/s40735-022-00636-6>
23. Tasić ŽZ, Petrović Mihajlović MB, Radovanović MB, Simonović AT, Antonijević MM (2020) Experimental and theoretical studies of paracetamol as a copper corrosion inhibitor. *J Mol Liq*. <https://doi.org/10.1016/j.molliq.2020.114817>
24. Tasić ŽZ, Petrović Mihajlović MB, Radovanović MB, Simonović AT, Antonijević MM (2019) Ibuprofen as a corrosion inhibitor for copper in synthetic acid rain solution. *Sci Res* 9:14710. <https://doi.org/10.1038/s41598-019-51299-2>
25. Biswal J, Pant HJ, Sharma VK, Sharma SC, Gupta AK (2021) Evaluation of inhibition effect of poly vinyl pyrrolidone on corrosion of bronze in simulated acid rain using thin layer activation technique. *Nucl Inst Methods Phys Res B* 503:30–36. <https://doi.org/10.1016/j.nimb.2021.07.007>
26. Khan A, Amjad M, Saboon S (2019) GC-MS analysis and biological activities of *Thymus vulgaris* and *Mentha arvensis* essential oil. *Turk J Biochem* 44:388–396. <https://doi.org/10.1515/tjb-2018-0258>
27. Escobar A, Perez M, Romanelli G, Blustein G (2020) Thymol bioactivity: a review focusing on practical applications. *Arab J Chem* 13:9243–9269. <https://doi.org/10.1016/j.arabjc.2020.11.009>
28. Jannati N, Honarvar M, Gharachorloo M (2021) Extraction of thymol compound from *Thymus vulgaris* L. oil. *JMPB* 1:81–84. <https://doi.org/10.22092/JMPB.2020.351668.1252>
29. Gedikoğlu A, Sökmen M, Çivit A (2019) Evaluation of *Thymus vulgaris* and *Thymbra spicata* essential oils and plant extracts for chemical composition, antioxidant, and antimicrobial properties. *Food Sci Nutr* 7:1704–1714. <https://doi.org/10.1002/fsn3.1007>
30. Sas IT, Proks M, Păunescu V, Pînzaru I, Sas I, Coricovac D, Moacă A, Dehelean C (2019) Thymus vulgaris extract formulated as cyclodextrin complexes: synthesis, characterization, antioxidant activity and in vitro cytotoxicity assessment. *Farmacia* 67:442–451. <https://doi.org/10.31925/farmacia.2019.3.10>
31. Hemmati S, Joshani Z, Zangeneh A, Zangeneh M (2019) Green synthesis and chemical characterization of *Thymus vulgaris* leaf aqueous extract conjugated gold nanoparticles for the treatment of acute myeloid leukemia in comparison to doxorubicin in a leukemic mouse model. *Appl Organomet Chem* 34:5267. <https://doi.org/10.1002/aoc.5267>
32. Crespo Y, Sánchez L, Sol A, García-Quintana Y (2019) Evaluation of the synergistic effects of antioxidant activity on mixtures of the essential oil from *Apium graveolens* L., *Thymus vulgaris* L. and *Coriandrum sativum* L. using simplex-lattice design. *Heliyon* 5:01942. <https://doi.org/10.1016/j.heliyon.2019.e01942>
33. Abdelbassat H, Bouhlali EDT, Khouya T, Ramchoun M, Zegzouti Y, Alem C, Benlyas M (2019) Antioxidant, anti-inflammatory and anticoagulant activities of three Thymus species grown in southeastern Morocco. *Future J Pharm Sci* 5:4–11. <https://doi.org/10.1186/s43094-019-0005-x>
34. Afonso AF, Pereira OR, Cardoso SM (2020) Health-promoting effects of thymus phenolic-rich extracts: antioxidant, anti-inflammatory and antitumoral properties. *Antioxidants* 9:814–822. <https://doi.org/10.3390/antiox9090814>
35. ASTM G1-03 (2017) Standard practice for preparing, cleaning and evaluating corrosion test specimens, ASTM International, WestConshohocken
36. Fuchs-Godec R, Zerjav G (2015) Corrosion resistance of high-level-hydrophobic layers in combination with Vitam in E—(a-tocopherol) as green inhibitor. *Corros Sci* 97:7–16. <https://doi.org/10.1016/j.corsci.2015.03.016>
37. Verma DK, Khan F (2016) Green approach to corrosion inhibition of mild steel in hydrochloric acid medium using extract of spirogyra algae. *Green Chem Lett Rev* 9:52–60. <https://doi.org/10.1080/17518253.2015.1137976>

38. Ngobiri NC, Oguzie EE, Li Y (2015) Eco-friendly corrosion inhibition of pipeline steel using *Brassica oleracea*. Int J Corros 2015:1–9. <https://doi.org/10.1155/2015/404139>
39. Yaqo EA, Anee RA, Abdulmajeed MH, Tomi IHR, Kadhim MM (2019) Aminotriazole derivative as anti-corrosion material for Iraqi kerosene tanks: electrochemical, computational and the surface study. Chem Select 4:9883–9892. <https://doi.org/10.1002/slct.201902398>
40. Alkarim TA, Al-Azawi KF, Anee RA (2021) Anticorrosive properties of Spiramycin for aluminum in acidic medium. Int J Corros Scale Inhib 10:1168–1188. <https://doi.org/10.17675/2305-6894-2021-10-3-20>
41. Bentiss F, Bouanis M, Mernari B, Traisnel M, Vezin H, Lagrenee M (2007) Understanding the adsorption of 4H-1,2,4-triazole derivatives on mild steel surface in molar hydrochloric acid. Appl Surf Sci 253:3696–3704. <https://doi.org/10.1016/j.corsci.2012.03.036>
42. Free ML (2002) Understanding the effect of surfactant aggregation on corrosion inhibition of mild steel in acid medium. Corros Sci 44:2865–2870. [https://doi.org/10.1016/S0010-938X\(02\)00080-X](https://doi.org/10.1016/S0010-938X(02)00080-X)
43. Mareci D, Chelariu R, Rusu I, Melniciuc Puică N, Sutiman D (2010) Electrochemical behaviour of some religious artefacts in simulated acid rain. Eur J Sci 6:57–70
44. El Adnani Z, Mcharfi M, Sfaira M, Benzakour M, Benjelloun AT, Touhami ME (2013) DFT theoretical study of 7-R-3methylquinoxalin-2 (1H)-thiones (R=H; CH₃; Cl) as corrosion inhibitors in hydrochloric acid. Corros Sci 68:223–230. <https://doi.org/10.1016/j.corsci.2012.11.020>

Publisher's Note Springer Nature remains neutral with regard to jurisdictional claims in published maps and institutional affiliations.